



# Theoretical study on mechanical and electronic properties of ternary diborides $\text{Sc}_{0.5}\text{V}_{0.5}\text{B}_2$ , $\text{Sc}_{0.5}\text{Nb}_{0.5}\text{B}_2$ and $\text{Sc}_{0.5}\text{Ta}_{0.5}\text{B}_2$

Quanmin Xie <sup>a,b</sup>, Yingkang Yao <sup>a,b</sup>, Xuwen Liu <sup>a,b</sup>, Jinshan Sun <sup>a,b</sup>, Zheng Zhang <sup>d</sup>, Lei Chen <sup>a,b,c,\*</sup>

<sup>a</sup> State Key Laboratory of Precision Blasting, Jianghan University, Wuhan 430056, China

<sup>b</sup> Hubei Key Laboratory of Blasting Engineering, Jianghan University, Wuhan 430056, China

<sup>c</sup> College of Physics and Optoelectronic Technology, Baoji University of Arts and Sciences, Baoji 721016, China

<sup>d</sup> Sichuan Jiaoda Engineering Detection & Consulting Co.,Ltd, China



## ARTICLE INFO

### Keywords:

Transition-metal diborides  
Superhard material  
First-principles  
Ideal strength  
Electronic structure

## ABSTRACT

Owing to the high thermal stability and superior mechanical properties, the transition-metal (TM) diborides have been proved to be a class of promising hard materials used as protective films. In the present work, a new type of ternary diborides  $\text{Sc}_{0.5}\text{V}_{0.5}\text{B}_2$ ,  $\text{Sc}_{0.5}\text{Nb}_{0.5}\text{B}_2$  and  $\text{Sc}_{0.5}\text{Ta}_{0.5}\text{B}_2$  alloyed by doping the TM scandium into  $\text{VB}_2$ ,  $\text{NbB}_2$  and  $\text{TaB}_2$  are systematically investigated using first-principle density functional theory (DFT) calculations. These ternary systems all possess higher hardness of up to about 45 GPa relative to their parent binary diborides  $\text{ScB}_2$ ,  $\text{VB}_2$ ,  $\text{NbB}_2$  and  $\text{TaB}_2$ , suggesting they could be viewed as promising candidates of superhard materials. An improved structure searching approach was employed to explore the potential stable and metastable structures of them under the pressure of 0 ~ 100 GPa. The hexagonal  $\text{AlB}_2$ -type structure ( $P6/mmm$ ) was confirmed to be their ambient phase, which can retain the stability up to 100 GPa. Meanwhile, their ideal tensile and pure shear strengths all reached about 40 GPa, demonstrating their superhard nature. The origin of the enhanced mechanical properties of these ternary systems was resolved in details by electronic analysis at fundamental level. Thanks to the introduction of the Sc, the  $p$ - $d$  interactions between TM and B atoms are greatly enhanced. This remarkable enhancement of  $p$ - $d$  coupling hybridization together with the pure covalent B-B bonds results in their high hardness property.

## 1. Introduction

Transition-metal diborides (TMB<sub>2</sub>s) are a class of famous ceramics with ultrahigh temperature chemical stability, electrical conductivity, excellent mechanical properties and high thermal conductivity. These multifunctional properties of TMB<sub>2</sub>s make them possess potential applications at extreme conditions. Motivated by combination of these unique features, plenty of experimental and theoretical studies have been performed to explore and discover novel diborides with superior properties. Thanks to the pure covalent B-B bonds and strong interaction of  $p$ - $d$  hybridization between TM and born atoms, most of these diborides exhibit excellent mechanical properties, e.g.  $\text{TiB}_2$ ,  $\text{ZrB}_2$ ,  $\text{HfB}_2$ ,  $\text{VB}_2$ ,  $\text{NbB}_2$ ,  $\text{TaB}_2$ ,  $\text{ReB}_2$ ,  $\text{OsB}_2$ , etc [1,2]. Among these TM diborides,  $\text{ReB}_2$  has been reported to possess 48 GPa hardness value under a 0.49 N load, which was the hardest diborides ever reported [3].  $\text{OsB}_2$  is also well known for its ultra-incompressibility with a high hardness of up to about 38 GPa [4]. The early TMB<sub>2</sub> (e.g.  $\text{TiB}_2$ ,  $\text{ZrB}_2$ ,  $\text{HfB}_2$ ,  $\text{VB}_2$ ,  $\text{NbB}_2$  and  $\text{TaB}_2$ )

prefer the  $\text{AlB}_2$ -type hexagonal structure ( $P6/mmm$ , No. 191), whereas the late TMB<sub>2</sub> (e.g.  $\text{ReB}_2$  and  $\text{OsB}_2$ ) adopt another hexagonal structure with the space group of  $P6_3/mmc$  (No. 194). These two structures are all comprised of alternating stacking of boron hexagons with covalent B-B bonds and metal layers in the hexagonal shaped unit cells. The difference of them is that the boron hexagons in  $P6/mmm$  structure are flat where they change to be puckered in  $P6_3/mmc$  structure. Additionally, most of these diborides can be synthesized at ambient conditions resulting in the lower synthesis cost relative to the pure covalent compounds such as diamond and cubic boron nitride, which is beneficial to their engineering application.

In recent years, some researchers have tried to introduce additional TM elements into binary carbides, nitrides or borides to form a new type of multi-element compounds for achieving the enhanced mechanical properties, e.g. hardness, strength as well as toughness [4–11]. According to the element doping, it can be expected to form two types of multi-element systems. The first is disordered solid solutions which are

\* Corresponding author at: State Key Laboratory of Precision Blasting, Jianghan University, Wuhan 430056, China.

E-mail addresses: [leichen@bjwlxy.edu.cn](mailto:leichen@bjwlxy.edu.cn), [stonley@163.com](mailto:stonley@163.com) (L. Chen).

so-called high entropy phase of these compounds. The second is ordered structures with definite crystalline configurations. Both of these two multinary systems are greatly affected by the kind of doping elements in the mechanical properties, which can be ascribed to the involved change of valence electron concentration (VEC). It was reported that when the VEC is about 8.4, the multinary carbides with their disordered high entropy phase possess the highest hardness. Meanwhile, the increasing VEC can lead to a significant change of the electronic structures which determine the bonding nature between the TM elements and the carbon atoms [5,6]. For the multinary nitrides, there exit the analogous effects of the VEC on the electronic structures and the macroscopically mechanical properties. In the disordered  $Ti_{0.5}W_{0.5}N$  systems, the introduction of the TM tungsten generating the change of balance of  $p$ - $d$  interactions (between TM and nitrogen atoms) and the metallic  $d$ - $d$  bonding states (between TM and TM atoms) causes the enhanced toughness [7]. In addition, our previous study about the ordered  $Ti_{0.5}W_{0.5}N$  system has proposed the VEC tuning effects on the electronic structures and the mechanical properties [8]. This VEC tuning method has also been used in the investigation of multinary borides such as  $Zr_{0.5}Sc_{0.5}B_2$ ,  $Zr_{0.5}Ti_{0.5}B_2$ ,  $Zr_{0.5}V_{0.5}B_2$ ,  $Ti_{0.5}Sc_{0.5}B_2$ ,  $Ti_{0.5}V_{0.5}B_2$ ,  $W_{0.5}Ta_{0.5}B$  [9,10] as well as other monoborides or diborides [11–16]. Liang et al. have found an anomalous hardening behavior of a class of TM monoborides (TMBs) exhibiting close relations between hardness and VEC. They have proposed that the optimum VEC of TMBs is about 8 electrons per formula unit. This hardening effect induced by the VEC tuning is mainly ascribed to the change of the electronic structures near the Fermi level ( $E_F$ ) [17]. Despite lots of interesting experimental or theoretical results on the physical properties for these binary and ternary  $AlB_2$ -type diborides, the investigations for the VEC tuning induced variation of mechanical behavior as well as the underlying atomistic mechanism are limited and insufficient. Therefore, it is desirable and fascinating to study the microscopic mechanism of the enhanced mechanical properties in association with the VEC tuning. Motivated by these previously reported findings based on the VEC tuning method, we firstly continued performing systematic study on the structural, mechanical and electronic properties of ternary diborides  $Sc_{0.5}V_{0.5}B_2$ ,  $Sc_{0.5}Nb_{0.5}B_2$  and  $Sc_{0.5}Ta_{0.5}B_2$  by doping Sc into the binary diborides ( $VB_2$ ,  $NbB_2$  and  $TaB_2$ ) to further explore the VEC tuning effects and underlying mechanism of the enhanced mechanical properties. For the  $p$ - $d$  hybridization of the TM-B, the introduction of Sc can reduce the valance electrons to 8 if the  $s$ -electrons are not taken into consideration because of its negligible contribution to the TM-B bonding interactions. This may lead to an optimization of electronic structure near the  $E_F$ , which is discussed detailedly in the electronic properties in this paper.

In the present work, an improved structure searching method of Crystal structure AnaLYsis by Particle Swarm Optimization (CALYPSO) has been employed to search the potential stable and metastable structures of these ternary diborides under the pressure of 0 ~ 100 GPa. Detailed mechanical properties containing ideal strengths, elastic moduli, as well as the elastic and strength anisotropies were studied. As expected, these ternary systems all possess higher hardness of up to about 45 GPa relative to their parent binary diborides  $ScB_2$ ,  $VB_2$ ,  $NbB_2$  and  $TaB_2$ , meaning they were promising candidates of superhard materials (Vicker's hardness is larger than 40 GPa in SI unit). The electronic structures were analyzed in depth and compared with their parent diborides to explore the underlying mechanism of the VEC tuning effects.

## 2. Calculation details

The TM scandium is introduced into the binary  $VB_2$ ,  $NbB_2$  and  $TaB_2$  such that the VEC is tuned as 10 per f.u. which should be corrected to be 8 per f.u. if the  $s$ -orbital electrons of TM atoms are not taken into consideration due to its little contribution to the  $p$ - $d$  covalent interactions. This VEC of 8 per f.u. is identical to the optimum value of monoborides as mentioned above. The structure searching was carried

out using the CALYPSO method [18,19] under the pressure of 0 GPa, 25 GPa, 50 GPa, 75 GPa and 100 GPa, respectively. The original structures are generated randomly with constraint of symmetry. Then, after local structural optimization, CALYPSO code sorts the structures by enthalpies and generates the new structures by particle swarm optimization for iterations. After sufficient cycles, the optimal structure possessing the minimum formation enthalpy can be obtained. The crystal cell is set as containing 1–4 f.u. For each structure searching pressure, there are 50 steps contained 40% new structures and 60% inherited structures. All the rest calculations containing structure optimization, phonon spectra, elastic moduli, ideal strengths, and electronic structure were performed through DFT projector augmented wave potentials (PAW) [20,21] within the generalized gradient approximation (GGA) [22]. The valence electrons were  $3p^63d^14s^2$  for Sc,  $3p^63d^34s^2$  for V,  $4p^64d^45s^1$  for Nb and  $5p^65d^36s^2$  for Ta. The Perdew-Burke-Ernzerhof (PBE) parametrization was used as the exchange and correlation functional, as implemented in the Vienna ab initio simulation package (VASP) [23]. The plane-wave basis set with the cutoff energy of 600 eV and the G-centered  $k$ -point meshes [24] of  $11 \times 11 \times 9$  (for  $ScB_2$ ,  $VB_2$ ,  $NbB_2$  and  $TaB_2$  within  $P6/mmm$  structure) and  $11 \times 11 \times 5$  (for ternary  $Sc_{0.5}V_{0.5}B_2$ ,  $Sc_{0.5}Nb_{0.5}B_2$  and  $Sc_{0.5}Ta_{0.5}B_2$ ) were adopted for ensuring the high accuracy of the calculations. The phonon spectra were calculated using the density functional perturbation theory (DFPT) method executed in the PHONOPY code [25]. The elastic moduli were evaluated in the Voigt-Reuss-Hill (VRH) approximation [26]. The empirical formula was used in calculating the Vickers hardness [27]. Crystal orbital Hamiltonian population (COHP) implemented in the LOBSTER code [28] was used in the bonding analysis. The electron localization function (ELF) [29] was also calculated for electronic analysis.

## 3. Results and discussions

### 3.1. Structural properties and stability

Structure prediction simulations of these ternary diborides together with their parent diborides containing 1–4 f.u. were firstly carried out through the CALYPSO method at various pressures of 0–100 GPa. These structure searches have not involved any experimental information. As expected, these ternary and binary diborides all adopt the hexagonal  $AlB_2$ -type structure with space group of  $P6/mmm$  No.191. It can be seen the two different TM elements occupy the metal layers alternately and the flat boron hexagons are among the TM layers (Fig. 1). The boron atoms have three nearest neighbor of boron atoms in each graphite-like plane and they are all arranged corners of the hexagons. The TM atoms are located at the center of octahedrons formed by the 12 boron atoms in the adjacent layers. The TM atoms occupy the  $1a$  (0, 0, 0) and the boron atoms occupy the  $2d$  (1/3, 2/3, 1/2) Wyckoff sites, respectively. The geometry optimized lattice parameters together with the previously theoretical and experimental values of various diborides are listed in Table 1. One can see our calculated results are close to the experimental values and the calculated results given from Ref. [30] and Ref. [31], demonstrating the high reliability of our calculations. It is to be noted that the lattice constants of these ternary diborides are very close to the mean values of their parent binary diborides, despite the existence of different VEC values. As is known, it is important to check the thermodynamic stability and the possibility of experimental synthesis for a new predicted material. We calculated formation enthalpies of these ternary diborides from the equation:  $H_f = \frac{1}{3}(H_{Sc_{0.5}M_{0.5}B_2} - \frac{1}{2}H_M - \frac{1}{2}H_{Sc} - 2H_B)$ , where  $H_{Sc_{0.5}M_{0.5}B_2}$ ,  $H_M$ ,  $H_{Sc}$  and  $H_B$  are the total enthalpies per atom (eV/atom) of these ternary diborides, TMs ( $bcc$ -V,  $bcc$ -Nb,  $bcc$ -Ta),  $hcp$ -Sc and  $\alpha$ -boron (in  $R\bar{3}m$  spacegroup). As presented in Table 1, the calculated formation enthalpies of these ternary diborides are all negative, demonstrating their thermodynamic stabilities. In consideration of the possibility of decomposition into their parent binary diborides, the relative enthalpies of them were also calculated based on

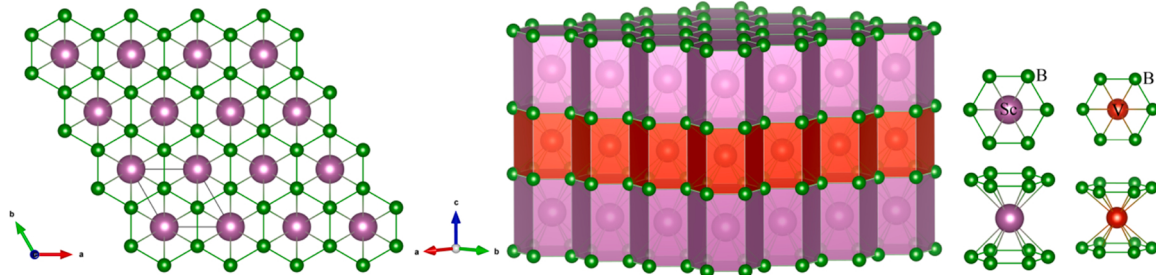


**Fig. 1.** Hexagonal  $P6/mmm$ -  $\text{Sc}_{0.5}\text{V}_{0.5}\text{B}_2$ . The large red, purple and small green spheres represent V, Sc, and B atoms respectively.

**Table 1**  
Calculated lattice parameters ( $\text{\AA}$ ), volume ( $\text{\AA}^3/\text{f.u.}$ ), formation enthalpy ( $H_f$ , eV/atom).

| Diborides                                  | Source              | $a$   | $c$   | Volume | $H_f$  |
|--|---------------------|-------|-------|--------|--------|
| $\text{ScB}_2$                             | This work           | 3.145 | 3.528 | 30.220 | -0.866 |
|  | Exp <sup>a</sup>    | 3.148 | 3.516 |        |        |
|  | Theory <sup>b</sup> | 3.139 | 3.521 |        |        |
| $\text{VB}_2$                              | This work           | 2.998 | 3.030 | 23.590 | -0.720 |
|  | Exp <sup>a</sup>    | 2.998 | 3.056 |        |        |
|  | Theory <sup>b</sup> | 2.992 | 3.027 |        |        |
| $\text{NbB}_2$                             | This work           | 3.114 | 3.350 | 28.130 | -0.696 |
|  | Exp <sup>a</sup>    | 3.115 | 3.265 |        |        |
|  | Theory <sup>b</sup> | 3.106 | 3.317 |        |        |
| $\text{TaB}_2$                             | This work           | 3.103 | 3.328 | 27.750 | -0.652 |
|  | Exp <sup>a</sup>    | 3.088 | 3.241 |        |        |
|  | Theory <sup>b</sup> | 3.132 | 3.358 |        |        |
| $\text{TiB}_2$                             | This work           | 3.033 | 3.226 | 25.710 | -1.059 |
|  | Exp <sup>a</sup>    | 3.038 | 3.220 |        |        |
|  | Theory <sup>b</sup> | 3.029 | 3.219 |        |        |
| $\text{Sc}_{0.5}\text{V}_{0.5}\text{B}_2$  | This work           | 3.035 | 3.310 | 26.410 | -0.814 |
| $\text{Sc}_{0.5}\text{Nb}_{0.5}\text{B}_2$ | This work           | 3.102 | 3.455 | 28.785 | -0.885 |
| $\text{Sc}_{0.5}\text{Ta}_{0.5}\text{B}_2$ | This work           | 3.090 | 3.439 | 28.430 | -0.905 |

<sup>a</sup> Ref. [30],

<sup>b</sup> Ref. [31].

the equation:  $\Delta H_f = \frac{1}{3}(H_{\text{Sc}0.5\text{M}0.5\text{B}2} - \frac{1}{2}H_{\text{ScB}2} - \frac{1}{2}H_{\text{MB}2})$ . The calculated  $\Delta H_f$  are  $-0.021$  eV/atom,  $-0.105$  eV/atom and  $-0.146$  eV/atom for  $\text{Sc}_{0.5}\text{V}_{0.5}\text{B}_2$ ,  $\text{Sc}_{0.5}\text{Nb}_{0.5}\text{B}_2$  and  $\text{Sc}_{0.5}\text{Ta}_{0.5}\text{B}_2$  respectively, suggesting they are more energetically favorable than their parent binary diborides.

The phonon dispersion curves as well as the density of states (PHDOS) are calculated through the supercell DFPT approach with linear response method to verify the dynamical stabilities of these ternary diborides within the  $\text{AlB}_2$  structure. The phonon dispersion curves and the corresponding total and projected DOS are plotted in Fig. 2. It is seen there are 18 branches in each phonon plot comprised of 15 optic and 3 acoustic branches with respect to behaving 6 atoms of the primitive cell. For the 3 acoustic branches, no soft mode can be observed, indicating the dynamical stabilities of these ternary diborides. It can be observed that the range of the phonon curves containing acoustic and optic branches has a little shift toward the lower frequency

from  $\text{Sc}_{0.5}\text{V}_{0.5}\text{B}_2$  to  $\text{Sc}_{0.5}\text{Nb}_{0.5}\text{B}_2$  and  $\text{Sc}_{0.5}\text{Ta}_{0.5}\text{B}_2$ , implying the descend trend of the atomistic interactions. The sharp peaks near the 25 THz frequency of the phonon DOS conform to the flat modes of the phonon spectra. The dominant contributions to the lower acoustic and partial optic branches come from the TM and Sc atoms, whereas the higher branches are mainly from the B-B interactions.

### 3.2. Mechanical properties

Ideal strength of crystalline materials plays an important role in determining the mechanical properties, such as macroscopic hardness, toughness, ductility [32–35]. Herein, first-principle method was employed to calculate the stress-strain relations by applying increasing tensile, compressive, shear and biaxial (Indentation shear strain) strains upon the crystal cells of these ternary and binary diborides. As is known,  $\text{VB}_2$  is magnetic experimentally, while the magnetic nature plays a negligible role in determining the mechanical properties [36]. Additionally, we found all the related systems in this work have the analogical results. Thus, the corresponding calculations have not taken the magnetic behavior into consideration. Fig. 3 illustrates the tensile/compressive stress-strain curves of the ternary diborides along the high symmetry  $[0001]$ ,  $[2\bar{1}\bar{1}0]$  and  $[1\bar{1}00]$  crystal directions.  $\text{Sc}_{0.5}\text{V}_{0.5}\text{B}_2$  possesses the lowest tensile strength of 42.2 GPa in the  $[0001]$  direction, indicating the  $(0001)$  plane is the easiest cleavage plane. The peak tensile strengths of  $[2\bar{1}\bar{1}0]$  and  $[1\bar{1}00]$  crystal directions can reach 66.5 GPa and 51.5 GPa, respectively. The corresponding strength anisotropy index ( $\sigma_{\max}/\sigma_{\min}$ ) is about 66.5 GPa / 42.2 GPa  $\approx 1.58$ . For  $\text{Sc}_{0.5}\text{Nb}_{0.5}\text{B}_2$  and  $\text{Sc}_{0.5}\text{Ta}_{0.5}\text{B}_2$  the tensile strengths along  $[0001]$ ,  $[2\bar{1}\bar{1}0]$  and  $[1\bar{1}00]$  directions are 40.2 GPa  $\sim$  41.5 GPa  $\sim$  61.3 GPa and 41.9 GPa  $\sim$  41.4 GPa  $\sim$  59.4 GPa, respectively. The corresponding strength anisotropy indexes are about 1.52 and 1.42. The analogical tensile strengths of these three ternary diborides can be ascribed to the identical VEC and the same crystal structure. Meanwhile, the largest tensile strengths of them are all exceeding 40 GPa, suggesting their superhard nature. The compressive strengths of them along the three crystal directions are all around 100 GPa, indicating they all have ultrahigh incompressibility. The calculated pure shear stress-strain relations are plotted in Fig. 4. As expected, the easiest cleavage ( $0001$ )

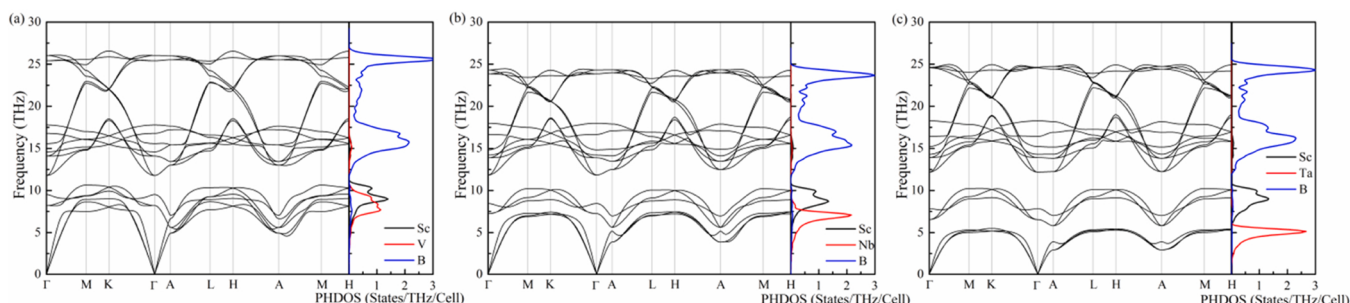


**Fig. 2.** Phonon dispersions of  $\text{Sc}_{0.5}\text{V}_{0.5}\text{B}_2$  (a),  $\text{Sc}_{0.5}\text{Nb}_{0.5}\text{B}_2$  (b), and  $\text{Sc}_{0.5}\text{Ta}_{0.5}\text{B}_2$  (c) at ambient pressure.

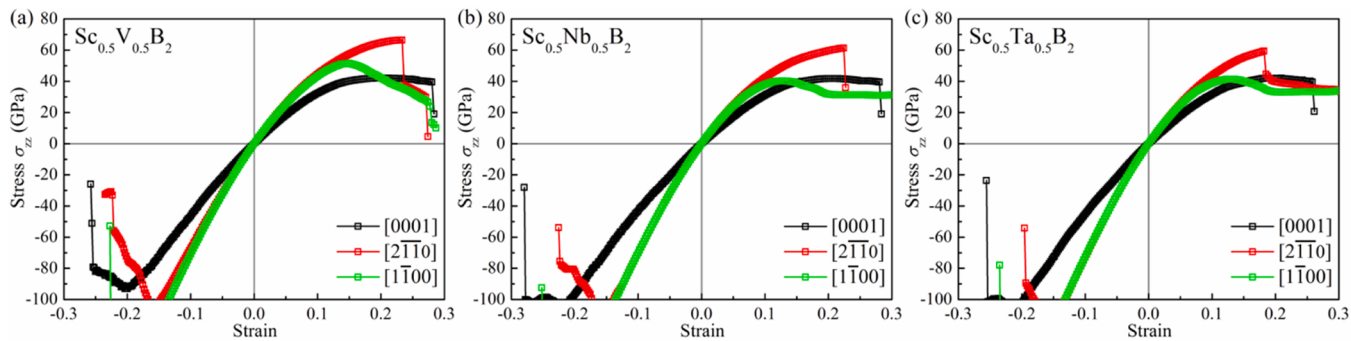


**Fig. 3.** Calculated tensile / compressive stress-strain curves of  $\text{Sc}_{0.5}\text{V}_{0.5}\text{B}_2$  (a),  $\text{Sc}_{0.5}\text{Nb}_{0.5}\text{B}_2$  (b), and  $\text{Sc}_{0.5}\text{Ta}_{0.5}\text{B}_2$  (c).

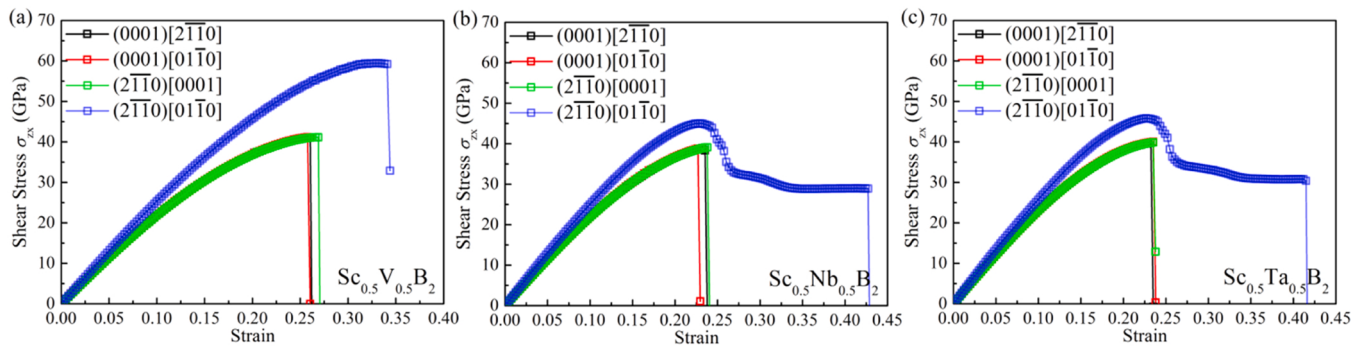


**Fig. 4.** Calculated shear stress-strain curves of  $\text{Sc}_{0.5}\text{V}_{0.5}\text{B}_2$  (a),  $\text{Sc}_{0.5}\text{Nb}_{0.5}\text{B}_2$  (b), and  $\text{Sc}_{0.5}\text{Ta}_{0.5}\text{B}_2$  (c).

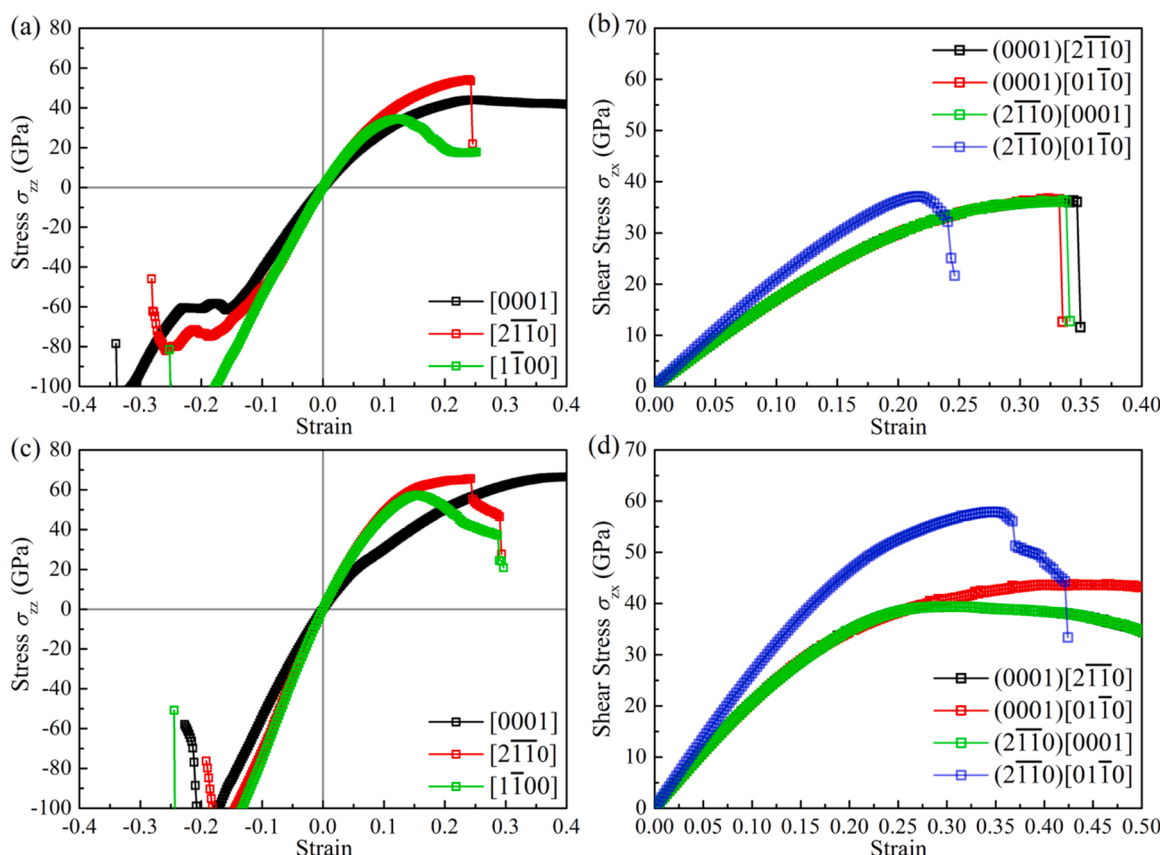


**Fig. 5.** Calculated tensile / compressive and shear stress-strain curves of  $\text{ScB}_2$  (a, b) and  $\text{VB}_2$  (c, d).

plane along  $[2\bar{1}\bar{1}0]$  and  $[01\bar{1}0]$  directions have the lowest peak stress of about 41 GPa for  $\text{Sc}_{0.5}\text{V}_{0.5}\text{B}_2$ . The highest peak strength is about 60 GPa along the  $(2\bar{1}\bar{1}0)[01\bar{1}0]$  slip direction, occurring at the strain of 0.33. For  $\text{Sc}_{0.5}\text{Nb}_{0.5}\text{B}_2$  and  $\text{Sc}_{0.5}\text{Ta}_{0.5}\text{B}_2$ , the lowest peak strengths are also about 40 GPa and the highest peak strengths are about 45 GPa. It can be seen  $\text{Sc}_{0.5}\text{V}_{0.5}\text{B}_2$  with the  $\sigma_{\max}/\sigma_{\min}$  value of about 1.46 exhibits a little more strength anisotropy relative to  $\text{Sc}_{0.5}\text{Nb}_{0.5}\text{B}_2$  and  $\text{Sc}_{0.5}\text{Ta}_{0.5}\text{B}_2$ , whose  $\sigma_{\max}/\sigma_{\min}$  values are about 1.13. The ideal strengths of binary  $\text{ScB}_2$  and  $\text{VB}_2$  are also calculated for comparison. As plotted in Fig. 5(a),  $\text{ScB}_2$  has the lowest tensile strength of about 34 GPa along  $[1\bar{1}00]$  direction and the largest peak tensile stress of 55 GPa along  $[2\bar{1}\bar{1}0]$  direction, which are all much smaller than the ternary diborides. Fig. 5(b) presents the pure shear stress-strain curves of  $\text{ScB}_2$ . It can be seen the peak strengths of the three selected crystal directions are all around 35 GPa, also smaller than the ternary diborides. Fig. 5(c, d) illustrates the stress-strain relations of binary  $\text{VB}_2$ . Though it has the larger tensile strength of about 57 GPa in the  $[1\bar{1}00]$  direction, the pure shear peak stress of the  $(2\bar{1}\bar{1}0)[0001]$  slip direction is only 39 GPa, which is much smaller than the ternary diborides. From the discussions above, one can conclude that the introduction of the additional scandium element can greatly improve the ideal strength of these diborides.

As is known, elastic constants play a significant role in determining the mechanical properties by the response of the crystal material to the external applied forces in the elastic limit, as indexed by the modulus and Poisson's ratio of the material. In the present work, the elastic constants of  $\text{AlB}_2$ -type diborides consist of five independent  $C_{ij}$  ( $C_{11}$ ,  $C_{33}$ ,  $C_{44}$ ,  $C_{12}$ ,  $C_{13}$ ). The calculated elastic constants as well as the corresponding elastic moduli together with the previous results are presented in Table 2. It can be seen the calculated elastic constants are highly consistent with the previous results, confirming the reliability of our calculations. The mechanical stability has also been checked using the criteria given by Ref. [37]. The elastic constants sufficiently satisfy the following criteria:

$$C_{44} > 0, C_{11} > |C_{12}|, (C_{11} + 2C_{12})C_{33} > 2C_{13}^2 \quad (1)$$

The calculated Hill elastic moduli,  $G/B$  ratio and Poisson's ratio  $\nu$  are also listed in Table 2.  $\text{ScB}_2$  has the lowest bulk and shear moduli, suggesting it has the smallest hardness and incompressibility. The other three binary diborides all possess a higher bulk modulus relative to the ternary diborides, which can be ascribed to the more valence electrons. However, it can be deduced that  $\text{NbB}_2$  and  $\text{TaB}_2$  have a weaker shear-resistant property by their smaller shear moduli than these ternary systems. Based on the elastic properties, we also evaluated the hardness of the binary and ternary diborides using the Chen empirical mode [27] as following:

$$H_v = 2(k^2 G)^{0.585} - 3 \quad (2)$$

The calculated Vickers hardness values are 42.1 GPa, 37.9 GPa, 26.6 GPa, 24.8 GPa, 45.3 GPa, 44.9 GPa and 44.3 GPa for  $\text{ScB}_2$ ,  $\text{VB}_2$ ,  $\text{NbB}_2$ ,  $\text{TaB}_2$ ,  $\text{Sc}_{0.5}\text{V}_{0.5}\text{B}_2$ ,  $\text{Sc}_{0.5}\text{Nb}_{0.5}\text{B}_2$  and  $\text{Sc}_{0.5}\text{Ta}_{0.5}\text{B}_2$ , respectively. It can be seen these ternary diborides all have the larger hardness than the binary diborides. Thus, the introduction of scandium can lead to the mediated balance of bulk and shear moduli as well as greatly improved hardness.

For these diborides, the microcracking can be easily induced because of the existence of the elastic anisotropy in the engineering applications. Thus, the elastic anisotropy of the ternary diborides is investigated to further understand its mechanical properties. Because of the similar bond distribution and the identical crystal symmetry for these diborides, the elastic anisotropies of them are almost the same with each other. Here, we take  $\text{Sc}_{0.5}\text{V}_{0.5}\text{B}_2$  as an example to analyze their elastic anisotropies. Based on the following equations [38], the Young's and shear moduli along random directions can be calculated and the results are plotted in Fig. 6.

$$E^{-1} = s_{11}(1 - l_3^2)^2 + s_{33}l_3^4 + (2s_{13} + s_{44})l_3^2(1 - l_3^2) \quad (3)$$

$$\begin{aligned} G^{-1} = & 4(4s_{12} + s_{11} - s_{22})l_1l_2m_1m_2 + 4[2s_{13} - (s_{22} + s_{33} - s_{44})]l_2l_3m_2m_3 \\ & + 4[2s_{13} - (s_{11} + s_{33} - s_{44})]l_1l_3m_1m_3 + s_{44}(l_2m_3 - l_3m_2)^2 \\ & + s_{44}(l_3m_1 - l_1m_3)^2 + 2(s_{11} - s_{12})(l_1m_2 - l_2m_1)^2 \end{aligned} \quad (4)$$

$$l = \begin{pmatrix} \sin \theta \cos \varphi \\ \sin \theta \sin \varphi \\ \cos \theta \end{pmatrix}, m = \begin{pmatrix} \cos \theta \cos \varphi \cos \chi - \sin \varphi \sin \chi \\ \cos \theta \sin \varphi \cos \chi - \cos \varphi \sin \chi \\ -\sin \theta \cos \chi \end{pmatrix}$$

Where  $S_{ij}$  ( $= C_{ij}^{-1}$ ) are elastic compliance constants and  $l_1$ ,  $l_2$ ,  $l_3$  are direction cosines. As plotted in Fig. 6(a, b), the three-dimensional (3D) distributions of directional dependence of Young's modulus and the corresponding cross sections in  $ab$  ( $xy$ ),  $bc$  ( $yz$ ) and  $ac$  ( $xz$ ) crystal planes are showcased. The 3D surface in Fig. 6(a) represents Young's modulus along various crystal directions. It can be seen that  $\text{Sc}_{0.5}\text{V}_{0.5}\text{B}_2$  has a non-spherical shape of the directional Young's modulus with a perfect circle appearing in  $ab$  ( $xy$ ) plane and an oval feature appearing in  $bc$  ( $yz$ ) and  $ac$  ( $xz$ ) planes, demonstrating its elastic anisotropy. The largest Young's modulus ( $E_{\max}$ ) appears in the  $ab$  ( $xy$ ) plane with the value of 577.5 GPa and the smallest Young's modulus ( $E_{\min}$ ) is in the  $bc$  ( $yz$ ) and  $ac$  ( $xz$ ) planes along  $[0001]$  direction with the value of 404.2 GPa. The anisotropy index can be expressed by the ratio of  $E_{\max} / E_{\min} \approx 1.43$ , which is much less than most of the typical NaCl-type TM nitrides and carbides as exhibited in our previous work [39,40]. The directional

**Table 2**

Calculated elastic constants ( $C_{ij}$ , GPa), bulk modulus ( $B$ , GPa), shear modulus ( $G$ , GPa), Young's modulus ( $E$ , GPa), Poisson's ratio  $\nu$ ,  $G/B$  ratio.

|  | Source              | $C_{11}$ | $C_{33}$ | $C_{44}$ | $C_{12}$ | $C_{13}$ | $B$ | $G$ | $E$ | $\nu$ | $G/B$ |
|--|---------------------|----------|----------|----------|----------|----------|-----|-----|-----|-------|-------|
| $\text{ScB}_2$                             | This work           | 500      | 382      | 182      | 51       | 63       | 192 | 196 | 439 | 0.12  | 1.02  |
|  | Theory <sup>a</sup> | 498      | 370      | 181      | 41       | 66       | 188 | 196 | 436 | 0.11  | 1.04  |
|  | Theory <sup>b</sup> | 497      | 362      | 184      | 43       | 13       |     |     |     |       |       |
| $\text{VB}_2$                              | This work           | 680      | 481      | 225      | 120      | 126      | 284 | 241 | 564 | 0.17  | 0.85  |
|  | Theory <sup>c</sup> | 683      | 462      | 229      | 111      | 127      | 284 | 247 |     |       | 0.87  |
|  | Theory <sup>b</sup> | 674      | 472      | 228      | 117      | 130      |     |     |     |       |       |
| $\text{NbB}_2$                             | This work           | 592      | 413      | 218      | 105      | 197      | 287 | 202 | 491 | 0.22  | 0.70  |
|  | Theory <sup>c</sup> | 608      | 494      | 193      |          | 193      | 299 | 220 | 542 | 0.22  | 0.74  |
|  | Theory <sup>b</sup> | 601      | 437      | 220      | 107      | 185      |     |     |     |       |       |
| $\text{TaB}_2$                             | This work           | 600      | 434      | 224      | 132      | 211      | 303 | 203 | 497 | 0.23  | 0.67  |
|  | Theory <sup>b</sup> | 591      | 468      | 218      | 166      | 175      |     |     |     |       |       |
| $\text{Sc}_{0.5}\text{V}_{0.5}\text{B}_2$  | This work           | 604      | 434      | 236      | 69       | 100      | 240 | 237 | 535 | 0.13  | 0.98  |
| $\text{Sc}_{0.5}\text{Nb}_{0.5}\text{B}_2$ | This work           | 593      | 417      | 237      | 59       | 107      | 237 | 234 | 528 | 0.13  | 0.98  |
| $\text{Sc}_{0.5}\text{Ta}_{0.5}\text{B}_2$ | This work           | 619      | 441      | 250      | 67       | 121      | 254 | 243 | 553 | 0.14  | 0.96  |

<sup>a</sup> Ref. [41],

<sup>b</sup> Ref. [31],

<sup>c</sup> Ref. [42].

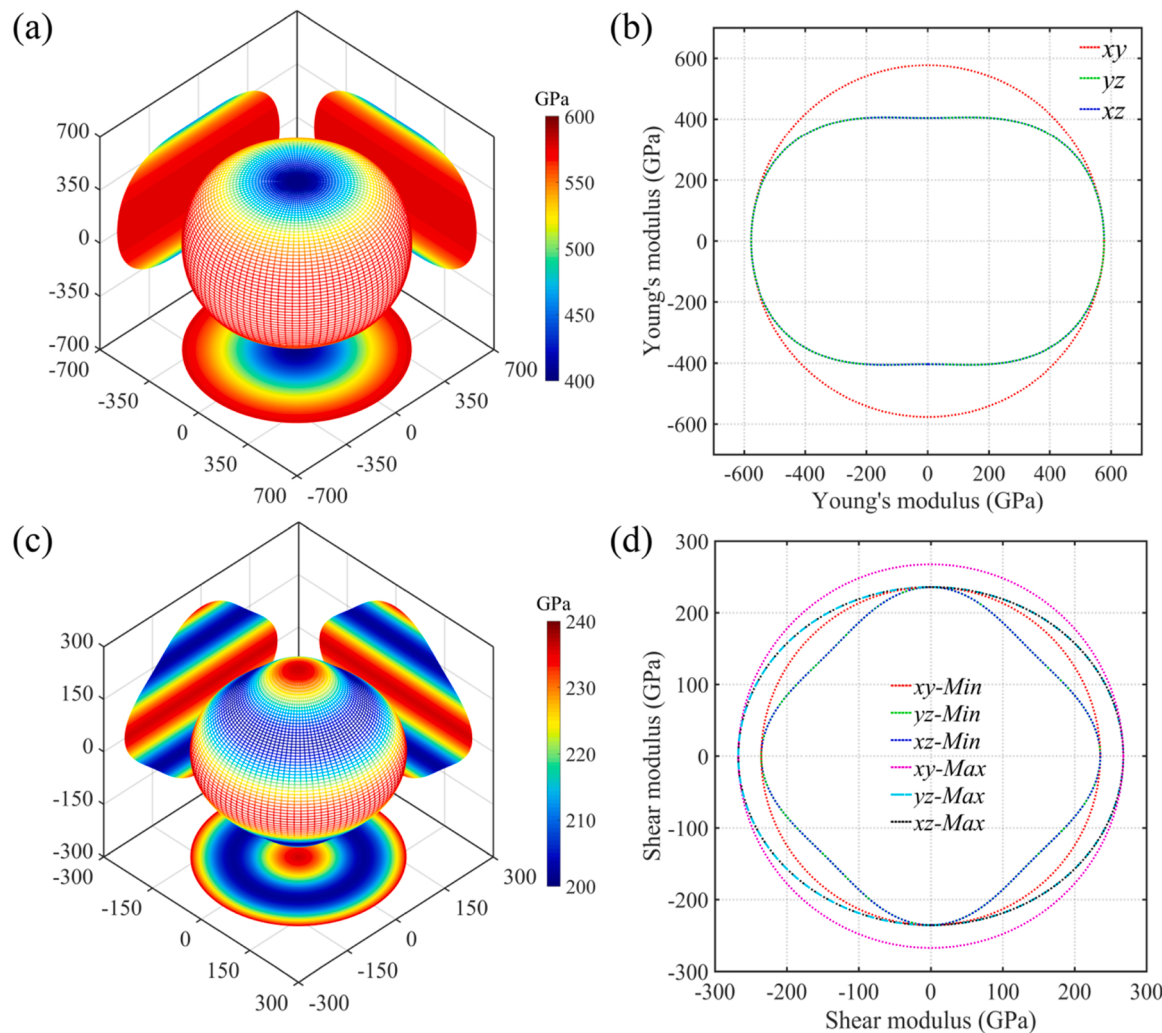


**Fig. 6.** Directional dependence of Young's modulus (a) with corresponding cross sections in ab (xy), bc (yz) and ac (xz) crystal planes (b) and directional dependence of minimum shear moduli (c) as well as cross sections of minimum and maximum shear moduli in ab (xy), bc (yz) and ac (xz) crystal planes for  $\text{Sc}_{0.5}\text{V}_{0.5}\text{B}_2$ .

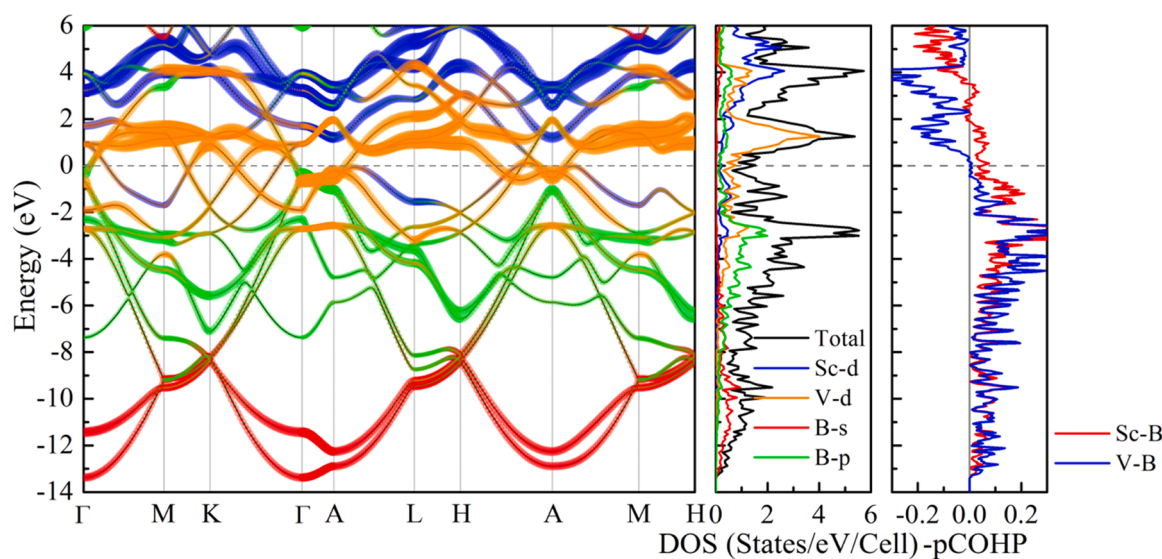


**Fig. 7.** Projected band structures, total and projected densities of states (t-DOS and p-DOS) as well as projected COHP for  $\text{Sc}_{0.5}\text{V}_{0.5}\text{B}_2$ . The blue, brown, red and green bubbles represent Sc-d, V-d, B-s and B-p respectively.

shear modulus is also calculated. As shown in Fig. 6(c, d), the 3D surface in Fig. 6(c) represents the minimum shear modulus along various directions in given crystal planes. The cross sections of the 3D surface of the minimum and maximum shear moduli in *ab* (*xy*), *bc* (*yz*) and *ac* (*xz*) crystal planes are showcased in Fig. 6(d). It is seen two perfect circles ( $G_{\max}$  and  $G_{\min}$ ) appearing in *ab* (*xy*) plane, and the anisotropy index of  $G_{\max} / G_{\min}$  are 264.4 GPa / 238.2 GPa  $\approx$  1.11. The *bc* (*yz*) and *ac* (*xz*) planes exhibit identical anisotropy with  $G_{\max} / G_{\min}$  of 264.4 GPa / 198.6 GPa  $\approx$  1.33. These results indicate this type of ternary diborides behave very little elastic anisotropy. The rest of two ternary diborides  $\text{Sc}_{0.5}\text{Nb}_{0.5}\text{B}_2$  and  $\text{Sc}_{0.5}\text{Ta}_{0.5}\text{B}_2$  have analogical elastic anisotropies, which are not shown here.

### 3.3. Electronic properties

As mentioned above, these ternary diborides possess enhanced ideal strengths and macroscopic hardness as well as little mechanical anisotropies relative to their parent binary diborides. Thus, in this section, let's turn to discuss their electronic properties to further understand the underlying mechanism at fundamental level. Fig. 7 shows the calculated projected band structures of  $\text{Sc}_{0.5}\text{V}_{0.5}\text{B}_2$  with spectral weight of *Sc-d*, *V-d*, *B-s* and *B-p* orbitals as well as the densities of states (DOS) and projected COHP. It can be seen  $\text{Sc}_{0.5}\text{V}_{0.5}\text{B}_2$  exhibits metallic character because of the absence of the band gap at  $E_F$ . It can be observed from the projected band structure that the valence bands are mostly composed of the mixture of the *Sc* / *V-d* *B-p*, and *B-s* orbitals, whereas the conduction bands are mostly composed of the *Sc* / *V-d* with a little contribution of *B-p* and *B-s* orbitals. From the band structure, it can be seen the strong coupling hybridization from *Sc* / *V-d* and *B-p* states in the range of  $-8 \sim 0$  eV, demonstrating the *p-d* interaction of *B* and *Sc* / *V*. This is agreement with the results of the density of states (DOS), also plotted in Fig. 7. Meanwhile, the pseudogap which is present just at the  $E_F$  can be obviously observed, implying the *p-d* bonding states are completely occupied while the anti-bonding states are not occupied. This can cause the improved electronic stability and the stronger TM-B interactions. The introduction of *Sc* substantially reduces the states near the  $E_F$ . The results of calculated COHP also confirmed this optimized *p-d* bonding interactions due to fact that the curves of *Sc-B* and *V-B* all exhibits bonding states below the  $E_F$ .  $\text{Sc}_{0.5}\text{Nb}_{0.5}\text{B}_2$  and  $\text{Sc}_{0.5}\text{Ta}_{0.5}\text{B}_2$  show the analogous behavior in their band structures and DOS plots as shown in Fig. 8 and Fig. 9. For comparison, we also calculated the projected band structures and DOS for the parent binary  $\text{ScB}_2$  and  $\text{VB}_2$  as plotted in Fig. 10 (a, b).

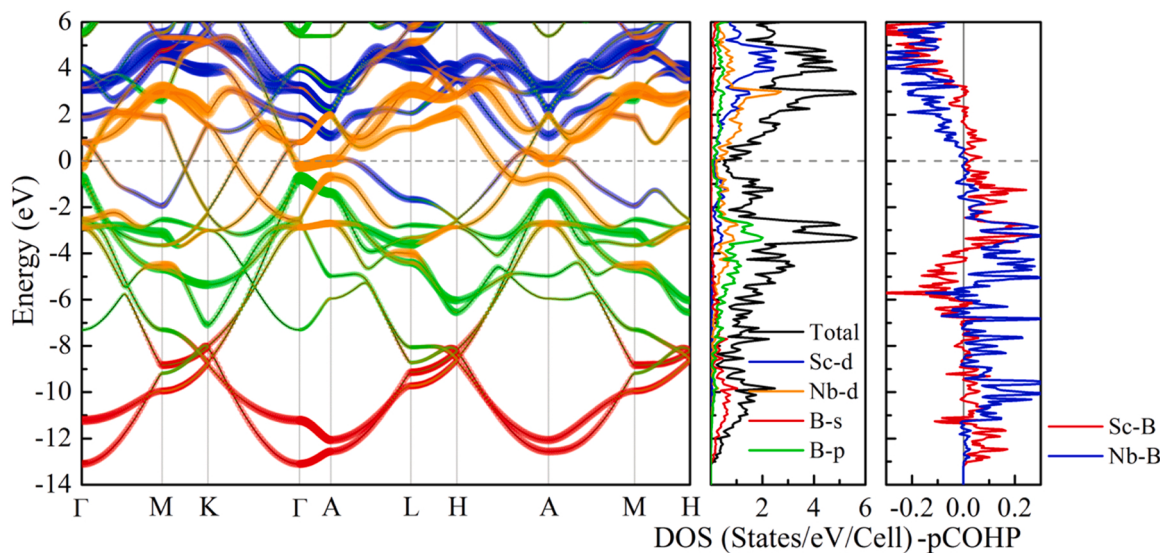


**Fig. 8.** Projected band structures, total and projected densities of states (t-DOS and p-DOS) as well as projected COHP for  $\text{Sc}_{0.5}\text{Nb}_{0.5}\text{B}_2$ . The blue, brown, red and green bubbles represent *Sc-d*, *Nb-d*, *B-s* and *B-p* respectively.

One can observe the clearly shift of the band dispersions toward the higher energy region for  $\text{ScB}_2$  and lower energy region for  $\text{VB}_2$ , resulting in the insufficient occupation of the bonding states and the excessive occupation of the anti-bonding states by the observation of relative location of  $E_F$  and pseudogap. Thus, the TM-B interactions are weakened compared to the ternary diborides. This optimization of the electronic structure may be the origin of the enhanced mechanical properties of the ternary diborides. The results of  $\text{Sc}_{0.5}\text{Nb}_{0.5}\text{B}_2$  and  $\text{Sc}_{0.5}\text{Ta}_{0.5}\text{B}_2$  as well as their parent diborides can be easily concluded by the results of  $\text{Sc}_{0.5}\text{V}_{0.5}\text{B}_2$  and its parent diborides because of the analogical VEC. This approach of improving hardness as well as strength by generating the multicomponent systems with optimized VEC is similar with the well-known eight-electron principle, which is used in light-element compounds such as diamond and *c*-BN to forming superhard nature. However, in these ternary TMB<sub>2</sub>s, the eight-electron principle is still applicable if the *s*-valence electrons of the TM atoms are not taken into consideration due to its little contribution to the TM-B bonding interactions.

The electronic localization function (ELF) for  $\text{Sc}_{0.5}\text{V}_{0.5}\text{B}_2$  is also calculated for further identifying the bonding nature of TM-B and B-B bonds. As shown in Fig. 11, the (11̄20) and (0001) planes are selected to examine the TM-B and B-B bonds. It can be seen there exists the charge localization between B atoms whereas it is absent between TM and B atoms, demonstrating the B-B bonds are strongly covalent and the TM-B bonds are weakly covalent. This type of TM-B bonds can be viewed as a mixture of metallic and covalent bonding whose covalent ingredients are responsible for the strong ideal strength and superhardness. The B-B bonds are purely covalent bonding like the C-C  $sp^3$  bonds in diamonds, which also provide great contributions to the strong macroscopic mechanical properties.

### 4. Conclusions

In summary,  $\text{Sc}_{0.5}\text{V}_{0.5}\text{B}_2$ ,  $\text{Sc}_{0.5}\text{Nb}_{0.5}\text{B}_2$  and  $\text{Sc}_{0.5}\text{Ta}_{0.5}\text{B}_2$  are systematically investigated using first-principle DFT calculations. These ternary diborides all possess the hardness of about 45 GPa, which is much higher than their parent binary diborides  $\text{ScB}_2$ ,  $\text{VB}_2$ ,  $\text{NbB}_2$  and  $\text{TaB}_2$ . Using the CALYPSO structure searching method, we explored the potential stable and metastable structures of them in the pressure of 0  $\sim$  100 GPa. We found the hexagonal AlB<sub>2</sub>-type structure (*P6/mmm*) can be confirmed as their ambient phase. This structure can retain its stability up to 100 GPa. Meanwhile, they all possess the high tensile and pure

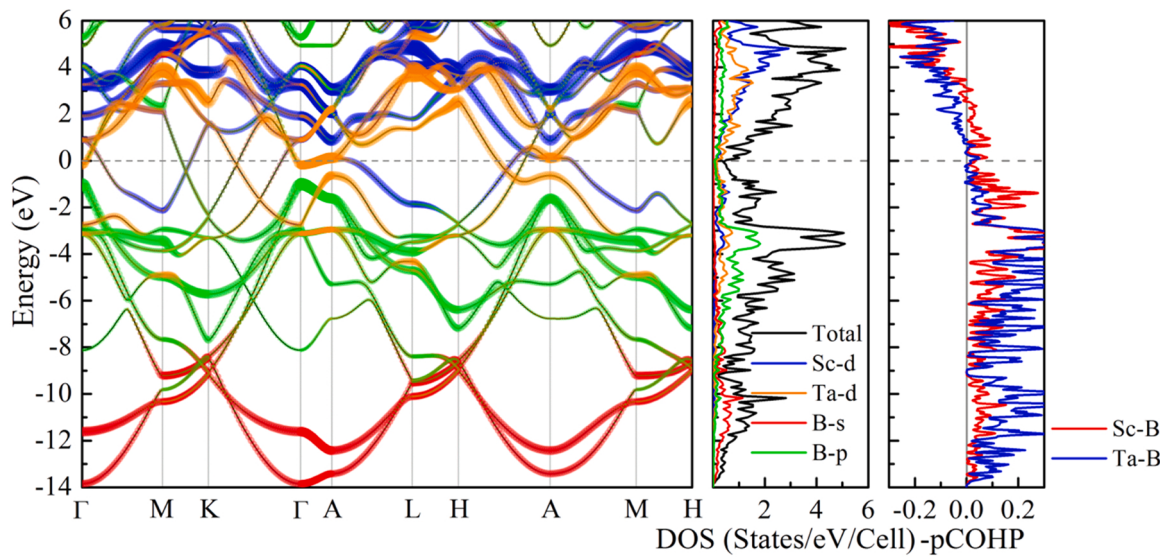


**Fig. 9.** Projected band structures, total and projected densities of states (t-DOS and p-DOS) as well as projected COHP for  $\text{Sc}_{0.5}\text{Ta}_{0.5}\text{B}_2$ . The blue, brown, red and green bubbles represent Sc-d, Ta-d, B-s and B-p respectively.

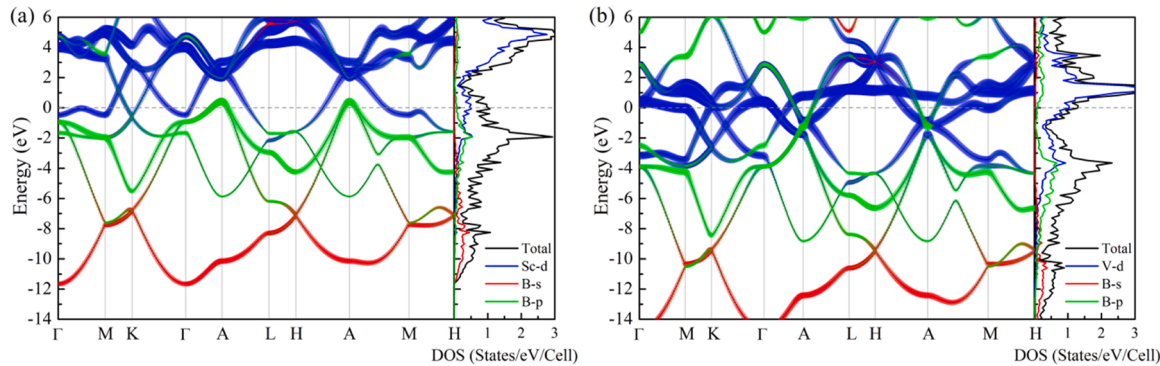


**Fig. 10.** Projected band structures, total and projected densities of states (t-DOS and p-DOS) for  $\text{ScB}_2$  (a) and  $\text{VB}_2$  (b).

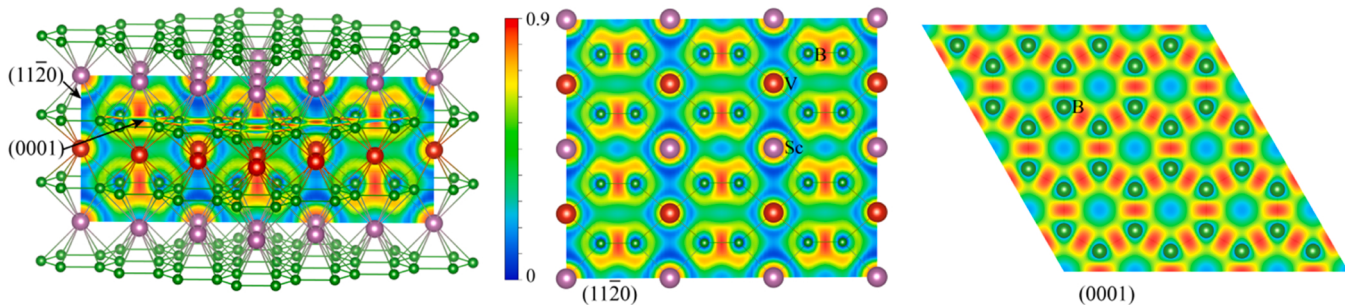


**Fig. 11.** Calculated ELF for  $\text{Sc}_{0.5}\text{V}_{0.5}\text{B}_2$  in  $(11\bar{2}0)$  and  $(0001)$  planes.

shear strengths of about 40 GPa, demonstrating their superhard nature. The origin of the enhanced mechanical properties of these ternary systems was resolved in details by electronic analysis at fundamental level. The introduction of the Sc leads to the great enhancement of the  $p-d$  interactions between TM and B. This  $p-d$  coupling hybridization together with the pure covalent B-B bonds results in their high hardness property.

#### CRediT authorship contribution statement

**Lei Chen:** Conceptualization, Methodology, Software, Data curation,

Investigation, Writing – original draft. **Quanmin Xie:** Supervision, Writing – review & editing. **Yingkang Yao:** Supervision, Writing – review & editing. **Xuwen Liu:** Supervision, Writing – review & editing. **Jinshan Sun:** Supervision, Writing – review & editing. **Zheng Zhang:** Supervision, Writing – review & editing.

#### Declaration of Competing Interest

The authors declare that they have no known competing financial interests or personal relationships that could have appeared to influence the work reported in this paper.

## Data Availability

No data was used for the research described in the article.

## Acknowledgments

This work was supported by State Key Laboratory of Precision Blasting and Hubei Key Laboratory of Blasting Engineering, Jianghan University (No. PBSKL2022D03), the Natural Science Foundation of China (Grant Nos. 51808554), the Natural Science Basic Research Plan in Shaanxi Province of China (Grant No. 2020JQ-892), Doctoral Research Start-up Fund Project (No. PBSKL-2022-QD-03).

## References

- [1] W.G. Fahrenholtz, G.E. Hilmas, I.G. Talmy, J.A. Zaykoski, Refractory diborides of zirconium and hafnium, *J. Am. Ceram. Soc.* 90 (5) (2007) 1347–1364.
- [2] Y.X. Wang, Elastic and electronic properties of  $TcB_2$  and superhard  $ReB_2$ : first-principles calculations, *Appl. Phys. Lett.* 91 (10) (2007), 101904.
- [3] H.-y Chung, Synthesis of ultra-incompressible superhard rhenium diboride at ambient pressure, *Science* 316 (2007) 436.
- [4] Y. Long, C. Zou, X. Zheng, H.T. Lin, F. Zhang, C. Wang, L. An, Effects of Re addition on phase stability and mechanical properties of hexagonal  $OsB_2$ , *J. Am. Ceram. Soc.* 101 (1) (2018) 151–158.
- [5] M.D. Hossain, S. Lowum, T. Borman, J.P. Maria, Fermi Lev. Eng. Mech. Prop. High. Entropy Carbides 2021 doi: 10.48550/arXiv.2101.04885.
- [6] K. Balasubramanian, S.V. Khare, D. Gall, Valence electron concentration as an indicator for mechanical properties in rocksalt structure nitrides, carbides and carbonitrides, *Acta Mater.* 152 (2018) 175–185.
- [7] D.G. Sangiovanni, L. Hultman, V. Chirita, I. Petrov, J.E. Greene, Effects of phase stability, lattice ordering, and electron density on plastic deformation in cubic TiWN pseudobinary transition-metal nitride alloys, *Acta Mater.* 103 (2016) 823–835.
- [8] L. Chen, J. Xu, M. Zhang, Y. Zhang, Theoretical study on structural, mechanical and electronic properties of ternary mononitride  $Ti_{0.5}W_{0.5}N$  from first-principles calculations, *Mater. Chem. Phys.* 242 (2020), 122476–122476.
- [9] E. Viswanathan, M. Sundareswari, D.S. Jayalakshmi, M. Manjula, Fermi surface and hardness enhancement study on ternary scandium and vanadium based borides by first principles investigation, *Comp. Mater. Sci.* 157 (2019) 107–120.
- [10] M. Zhang, H. Yan, Y. Zhang, Q. Wei, Mechanical strength and origin of the strengthening effect of tantalum in superhard  $W_{0.5}Ta_{0.5}B$  monoboride, *Ceram. Int.* 44 (9) (2018) 10463–10469.
- [11] F. Dai, Z. Feng, Y. Zhou, First-principles investigation on the chemical bonding, elastic properties and ideal strengths of MoAlB and WaIB nanolaminated MAB phases, *Comp. Mater. Sci.* 147 (2018) 331–337.
- [12] S. Aydin, M. Şimşek, Stability and superconductivity properties of metal substituted aluminum diborides ( $M_{0.5}Al_{0.5}B_2$ ), *Comp. Mater. Sci.* 154 (2018) 234–242.
- [13] S. Wang, Y. Pan, Y. Lin, C. Tong, Influence of doping concentration on mechanical properties of  $Mo_2FeB_2$  alloyed with Cr and Ni from first-principle calculations, *Comp. Mater. Sci.* 146 (2018) 18–25.
- [14] Y. Tu, Y. Wang, First-principles study of the elastic properties of  $Os_xW_{1-x}B_2$  and  $Re_xW_{1-x}B_2$  alloys, *Solid State Commun.* 151 (3) (2011) 238–241.
- [15] F. Lin, K. Wu, J. He, R. Sa, Q. Li, Y. Wei, Mixed-metal effects on ultra-incompressible metal diborides: Density functional computations, *Chem. Phys. Lett.* 494 (1–3) (2010) 31–36.
- [16] M. Matas, A. Farhadizadeh, J. Houska, Vacancies and substitutional defects in multicomponent diboride  $Ti_{0.25}Zr_{0.25}Hf_{0.25}Ta_{0.25}B_2$ : first-principle study, *J. Phys.: Condens. Matter* 34 (9) (2022), 095901.
- [17] Y. Liang, Z. Gao, P. Qin, L. Gao, C. Tang, The mechanism of anomalous hardening in transition-metal monoborides, *Nanoscale* 9 (26) (2017) 9112–9118.
- [18] Y. Wang, J. Lv, L. Zhu, Y. Ma, Crystal structure prediction via particle-swarm optimization, *Phys. Rev. B* 82 (9) (2010) 1–8.
- [19] Y. Wang, J. Lv, L. Zhu, Y. Ma, CALYPSO: a method for crystal structure prediction, *Comput. Phys. Commun.* (2012) 2063–2070.
- [20] Projector augmented-wave method *Phys. Rev. B* 50 24 1994 17953 17979.
- [21] G. Kresse, D. Joubert, From ultrasoft pseudopotentials to the projector augmented-wave method, *Phys. Rev. B* 59 (1999) 1758–1775.
- [22] J.P. Perdew, K. Burke, M. Ernzerhof, Generalized Gradient Approximation Made Simple, *Phys. Rev. Lett.* 77 (1996) 3865–3868.
- [23] G. Kresse, J. Furthmüller, Efficient iterative schemes for ab initio total-energy calculations using a plane-wave basis set, *Phys. Rev. B* 54 (1996) 11169–11186.
- [24] H.J. Monkhorst, J.D. Pack, Special points for Brillouin-zone integrations, *Phys. Rev. B* 13 (1976) 5188–5192.
- [25] A. Togo, I. Tanaka, First principles phonon calculations in materials science, *Scr. Mater.* 108 (2015) 1–5.
- [26] M. Born, K. Huang, *Dynamical Theory of Crystal Lattices*, Oxford University Press, Inc., London, 1954.
- [27] X.-Q. Chen, H. Niu, D. Li, Y. Li, Intermetallics Modeling hardness of polycrystalline materials and bulk metallic glasses, *Intermetallics* 19 (9) (2011) 1275–1281.
- [28] V.L. Deringer, A.L. Tchougr, R. Dronskowski, Crystal orbital hamilton population (COHP) analysis as projected from plane-wave basis sets, *J. Phys. Chem. A* 115 (2011) 5461–5466.
- [29] A.S.B. Silvi, Classification of chemical bonds based on topological analysis of electron localization functions, *Nature* 371 (1994) 683–686.
- [30] P. Vajeeston, P. Ravindran, C. Ravi, R. Asokamani, Electronic structure, bonding, and ground-state properties of AlB<sub>2</sub>-type transition-metal diborides, *Phys. Rev. B* 63 (2001), 045115.
- [31] Y. Zhou, H. Xiang, Z. Feng, Z. Li, General trends in electronic structure, stability, chemical bonding and mechanical properties of ultrahigh temperature ceramics  $TMB_2$  (TM = transition metal), *J. Mater. Sci. Technol.* 31 (3) (2015) 285–294.
- [32] C. Zhang, H. Sun, J.S. Tse, C. Chen, Indentation strength of ultraincompressible rhenium boride, carbide, and nitride from first-principles calculations, *Phys. Rev. B* 86 (2012), 014108.
- [33] Z. Pan, H. Sun, Y. Zhang, C. Chen, Harder than diamond: superior indentation strength of wurtzite BN and lonsdaleite, *Phys. Rev. Lett.* 102 (2009), 055503.
- [34] Z. Pan, H. Sun, C. Chen, Colossal Shear-Strength Enhancement of Low-Density Cubic BC<sub>2</sub>N by Nanoindentation, *Phys. Rev. Lett.* 98 (2007), 135505.
- [35] R.H. Telling, C.J. Pickard, M.C. Payne, J.E. Field, Theoretical strength and cleavage of diamond, *Phys. Rev. Lett.* 84 (2000) 5160–5163.
- [36] P. Wang, R. Kumar, E.M. Sankaran, X. Qi, X. Zhang, D. Popov, A.L. Cornelius, B. Li, Y. Zhao, L. Wang, Vanadium diboride (VB<sub>2</sub>) synthesized at high pressure: elastic, mechanical, electronic, and magnetic properties and thermal stability, *Inorg. Chem.* 57 (2018) 1096–1105.
- [37] K.H.M. Born, *Dynamical Theory of Crystal Lattices*, Oxford University Press, Inc., London, 1954.
- [38] T.C.T. Ting, *Anisotropic Elasticity Theory*, Oxford University Press, Inc., New York, 1996.
- [39] L. Chen, Z. Jiang, First-principles study on a new type of quaternary carbonitride VWCN with outstanding mechanical properties, *Int. J. Refract. Met. H.* 92 (2020), 105319–105319.
- [40] L. Chen, J. Xu, M. Zhang, Z. Wen, Z. Jiang, Structural, mechanical and electronic properties study on group 5 transition metals ternary mononitrides from first-principles calculations, *J. Alloy. Compd.* 813 (2020), 152246–152246.
- [41] A. Waśkowska, L. Gerward, J. Staun Olsen, K. Ramesh Babu, G. Vaitheeswaran, V. Kanchana, A. Svane, V.B. Filipov, G. Levchenko, A. Lyaschenko, Thermoelastic properties of ScB<sub>2</sub>, TiB<sub>2</sub>, YB<sub>4</sub> and HoB<sub>4</sub>: Experimental and theoretical studies, *Acta Mater.* 59 (12) (2011) 4886–4894.
- [42] I.R. Shein, A.L. Ivanovskii, Elastic properties of mono-and polycrystalline hexagonal AlB<sub>2</sub>-like diborides of s, p and d metals from first-principles calculations, *J. Phys.: Condens. Matter* 20 (41) (2008), 415218.